ACS OMEGA

Open Access

http://pubs.acs.org/journal/acsodf

Article

Molecular Dynamics Study on the Effect of Cyclic Conducting Moieties on Poly(2,6-dimethyl-1,4-phenylene oxide) Anion Exchange Membranes

Thabakgolo T. Letsau, Takuya Mabuchi,* and Phumlani F. Msomi*

Cite This: *ACS Omega* 2023, 8, 48711−48718

Read Online

ACCESS | Metrics & More | Article Recommendations | Supporting Information

ABSTRACT: We investigate PPO quaternized with different azoles (five-membered heterocyclic compounds) with a different odd number of Nitrogen atoms (1*N*-pyrrole, 3*N*-1,2,3-triazole, and 5*N*-pentazole) to form pyrrolium-PPO(py-PPO), 1,2,3,-triazolium-PPO(tri-PPO) and pentazolium-PPO(pen-PPO) AEMs, using molecular dynamics (MD) simulations to compare and evaluate their OH^- transport via the vehicular mechanism. OH^- diffusivity at the hydration level $\lambda = 12$ is 3.10×10^{-10} m^2/s, 1.92×10^{-10} m^2/s m^2/s, and 1.91×10^{-10} m^2/s for py-PPO, tri-PPO, and pen-PPO, respectively. This trend is due to the shorter distance between adjacent groups of py-PPO (7.5 Å) leading to an efficient hydroxide transport than tri-PPO (7.8 Å) and pen-PPO (8.1 Å) at $\lambda = 12$. Also, this trend is justified by the smaller average number of clusters for py-PPO (1.2), smaller than tri-PPO(2.0), and pen-PPO (1.5) at $\lambda = 12$, which suggests better connectivity and hence better conductivity.

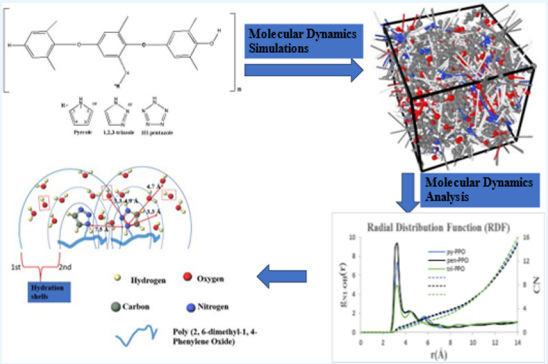

1. INTRODUCTION

Recently, research has been focused on finding ways to get energy from clean and renewable sources to help solve environmental problems and help us move toward a more sustainable energy development.[1] Polymer electrolyte membrane fuel cells have attracted significant attention in recent years, since they convert chemical energy into clean electrical energy with high efficiency. The two most studied fuel cells by experiments and Molecular Dynamics (MD) are the proton exchange membrane (PEM) and anion exchange membranes (AEM) fuel cells.[2]

The need for expensive Platinum (Pt) catalysts in PEM fuel cells is one of their main drawbacks. However, efforts have been made to reduce the costs of PEM fuels by reducing the Pt loading while improving or maintaining its performance; it is now clear that the only way we are going to see mass commercialization of the fuel cell technology is to shift our focus to other types of fuel cells which do not require Pt catalyst.[3,4]

AEM fuel cells have attracted much attention due to their nonutilization of Pt catalysts due to their alkaline environment, which has higher oxygen-reduction kinetics and high electro-oxidation kinetics, also allowing for greater flexibility of fuels, including Nitrogen based fuels. In addition, the electro-osmotic dragging force produced by the transportation of anions is in the opposite direction of the fuel; this reduces the fuel crossover.[1,5]

Despite the benefits of AEMs, their cationic group degradation in alkaline environments and low ion conductivities are the main drawbacks to their commercialization. In AEMs, the membranes are positively charged (e.g., $N^+(CH_3)_3$), and these membranes are immersed in an alkaline medium (KOH, NaOH, etc.) for hydroxide conductivity. So, the membranes need to be able to resist degradation by OH^- when they are immersed in this KOH. These cation groups are degraded due to Hofmann (or) E1 elimination reactions and nucleophilic substitution (Figures 1−3).[6,7]

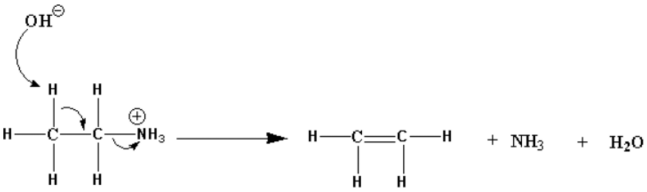

Figure 1. Hoffmann elimination degradation mechanism.

Received: July 21, 2023
Revised: November 2, 2023
Accepted: November 24, 2023
Published: December 12, 2023

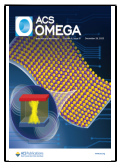

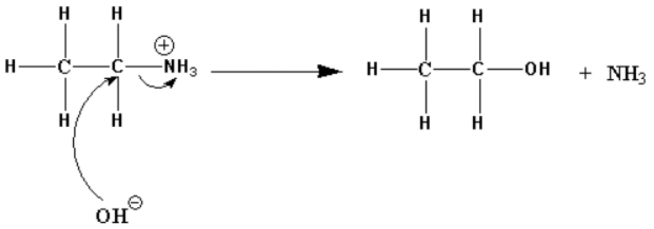

Figure 2. Direct nucleophilic substitution mechanism-pathway 1.

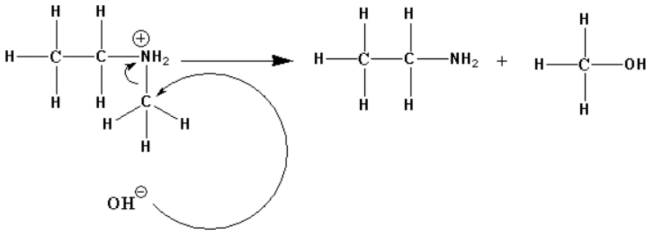

Figure 3. Direct nucleophilic substitution mechanism-pathway 2.

The polymer's backbone, type of cations, and the specific locations of the cations on the polymeric structure all affect how quickly the membrane degrades. To create a high-performance membrane, the polymer backbone, and any connected cations must exhibit high stability in an alkaline environment, even at high temperatures (60−80 °C).[7−10]

Polymer backbones with no electron-withdrawing groups on their structure, such as poly(phenylene oxide), are stable under alkaline conditions over polymer backbones with electron-withdrawing groups, such as poly(sulfone), since they are susceptible to OH^- attack and chain scissions.[8,11] High alkaline stable and hydroxide conductivity AEMs can be rationally designed once a suitable cationic group embedded or attached to a stable polymer backbone is identified.[9] Nitrogen-rich heterocycles of the azole family (pyrazole, pyrazoles, tetrazole, pentazoles, 1,2,3- and 1,2,4-triazole) are known to form long-range ion-conducting pathways.[12,13] PPO quaternized with 1,2,3-triazoles was reported by Li et al.,[14] to enhance OH^- transport in AEMs. The triazole enhanced anion transport by providing more sites for water and hydrogen to bond effectively and continuously. At 20 °C, OH^- conductivity of 27.8−62 mS/cm, alkaline stability in 1 M NaOH at 80 °C, and a peak power density of 188.7 mW/cm^2 at 50 °C, all higher than typical PPO.

Since OH^- is transferred through water channels, we believe that ionic conduction and alkaline stability through AEM strongly depend on the formation of water channels. The polymer electrolyte membrane's three-dimensional water channel network must first be constructed to improve ionic conduction. Molecular dynamics (MD) simulation effectively comprehends OH^- transport and alkaline stability in AEMs.[3,15] Previous MD simulations focused on the effect of different side chains based on the kind of ion they conduct (quaternary ammonium-functionalized anion exchange membrane and sulfonated proton exchange membrane) on their transport properties[3] and the effect of different substitutions around the same azole group on their OH^- transport and alkaline stability.[15] Still, the effect of different numbers of Nitrogens on the azole group has never been considered. Thus, it is necessary to study the effect of different azole groups on the same polymer to understand their effect on the OH^- transport and alkaline stability.

In this study, PPO was quaternized with different azoles (five-membered heterocyclic compounds) with a different odd number of Nitrogen atoms (1*N*-pyrrole, 3*N*-1,2,3-triazole, and 5*N*-pentazole) to form pyrrolium-PPO(py-PPO), 1,2,3,-triazolium-PPO(tri-PPO) and pentazolium-PPO(pen-PPO) AEMs, and MD simulations were used to investigate the effect on different azoles on OH^- transport and alkaline stability at various hydration levels. This work has not been reported before, and we are hopeful that these results will give theoretical guidance on the design of azole-based AEMs, which can be applied as a guide toward designing an AEM with good properties and water management in a practical setting.

We considered a vehicular mechanism (hydroxide ions attached to an oxygen and move together) for the transport of OH^- because the molecular dynamics cannot explain the Grotthuss mechanism (OH^- jumps from stationery oxygen to a neighboring oxygen atom that is in the right position with) since it does not allow changes in the chemical bonding topology. Also, a study by Chen et al.,[16] showed that vehicular diffusion contributes 80% of the total diffusion in OH^- transport, and Grotthuss diffusion contributes 20%. The alkaline stability was evaluated by the distribution of OH^-

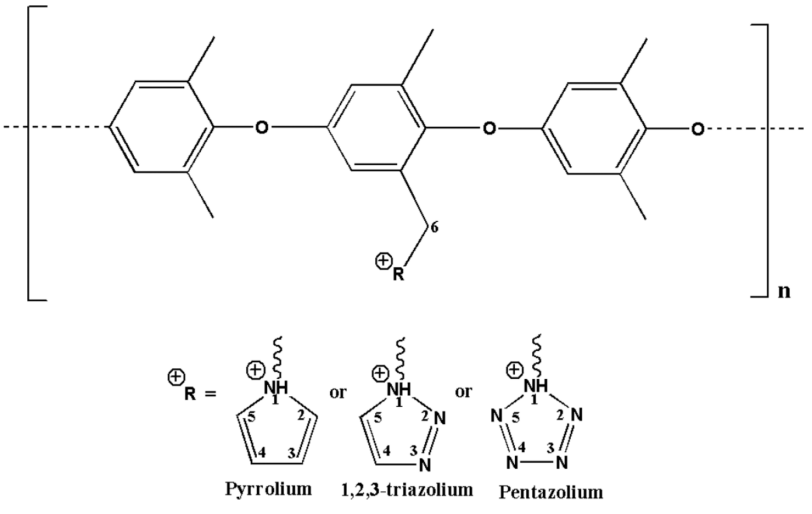

Figure 4. Chemical structure of azole quaternized PPO.

https://doi.org/10.1021/acsomega.3c05291
ACS Omega 2023, 8, 48711−48718

around different sites of each AEM structure and the hydration structure on each AEM. This provided theoretical guidance for the design of subsequent AEM structures.

2. SIMULATION METHODS

2.1. Molecular Model Construction. We assumed a poly(*p*-phenylene oxide) (PPO) quaternized with different cationic groups, as shown in the figure below in Figure 4. These Atomistic polymers were constructed, and their charges were manually assigned by ACPYPE (or AnteChamber PYthon Parser interfacE).

2.2. Computational Details. Molecular dynamics (MD) simulations using a mechanics force field were done using a Large-scale Atomic/Molecular Massively Parallel Simulator (LAMMPS) (64-bit) based on Dreiding force fields. A single homo polymer with 10 degrees of polymerization and both ends of the chain terminated with hydrogens was modeled using molecular modeling software called Winmostar. For a homo polymer cell builder, 4 QPPO chains were randomly placed in a cell with a three-dimensional periodic boundary condition. Each system contained an equal number of cationic quaternized PPO polymers with an equivalent number of OH^- and water molecules. The hydration level ($\lambda = 12$) was chosen to be the highest because, as shown in Figure S1, the D_{OH} increases from $\lambda = 3$ to $\lambda = 9$ significantly, but between $\lambda = 9$ and $\lambda = 12$, there is a small increase which shows that $\lambda = 12$ is the maximum amount of hydration level the system can maintain. Also, Wu et al.,[15] reported the same conditions. The initial density of 0.01 g/cm^3 was used for both hydration levels on all AEMs. Energy minimization was done to find a set of coordinates representing the minimum energy conformation for the given structure. The annealing procedure was carried out to eliminate the initial configurations and orientations of the molecules, establishing the stable equilibrium state: First, compression at high pressure (NPT, 300k, 100 atm) was done, and annealing for 1 ns at (NPT 300 K,1 atm, and NVT 800 K), repeated four times. Equilibration for 5 ns at NPT (300 K, 1 atm) after the annealing procedure was done to stabilize the equilibrium, and the final step, which is production, was run for ten ns at NVT (300 K) collected every 0.2 ps.[17,18] The details of the hydrated AEMs are summarized in Table 1.

Table 1. Comparison of Hydrated Membranes and Simulation Conditions

hydration level (λ)	3	12
polymer chain	4	4
number of cations (N^+)	40	40
number of hydroxide ions (OH^-)	40	40
number of water molecules (H_2O)	120	480

2.3. Simulation Analysis. To characterize the structural properties of AEMS, the radial distribution function (RDF) denoted by $g(r)$ and coordination number (CN) were evaluated. $g_{A\text{-}B}(r)$ describes the distribution of atom B surrounding atom A, which can be calculated using eq 1. CN calculates the number of molecules around a molecule of interest using eq 2.[1]

$$g_{A\text{-}B}(r) = \frac{dN_B}{\rho 4\pi r^2 dr} \quad (1)$$

$$CN = \int_0^r \rho 4\pi r^2 g(r) dr \quad (2)$$

where dN_B is the number of atoms B detected in a spherical shell of thickness dr with distance r to atom A and ρ denotes the average number density of atoms in the cell.

Self-diffusion coefficient of OH^- (D_{OH}) was calculated from the slope of the mean square displacement (MSD) as a function of simulation time according to the Einstein–Smoluchowski relation.[15]

$$D = \lim_{t\to\infty} \frac{1}{6N_m t} \sum_{i=1}^{N_m} MSD(t) = \lim_{t\to\infty} \frac{1}{6N_m t} \sum_{i=1}^{N_m} \langle |r \to (t) - r \to (0)|^2 \rangle \quad (3)$$

Where, $r \to (t)$ and $r \to (0)$ are the position vectors at times t and 0, respectively. N_m is the total number of molecules. From the self-diffusion coefficient, ion conductivity (σ) can be calculated using Nernst–Einstein equation.[15]

$$\sigma = D\frac{Nz^2e^2}{kT} \quad (4)$$

N is the number density of OH^-, z is the carrier charge, e is the elementary charge, k is the Boltzmann constant, and T is the absolute temperature.

Water Cluster analysis is a quantitative measure of structure with regard to connectivity and confinement. An Open Visual Tool (OVITO) was used to compute the cluster analysis. The oxygen–oxygen distance between water molecules and hydroxide ions in this study was set at 3.5 Å.[19]

3. RESULTS AND DISCUSSION

In this section, the D_{OH} of different azole-based groups, structural properties around the azole groups, and the water clusters were studied to understand the effect of different azole-based groups on OH^- transport.

3.1. Self-Diffusivity of OH^-. D_{OH} of Azole-based AEMS at different hydration levels is shown in Figure 5. Figure 5 shows the mean square displacement of OH^- ions, of which slopes directly indicate the diffusivities (D_{OH}) according to eq 3,[15] D_{OH} at $\lambda = 3$ is 1. 45 × 10^{-10} m^2/s, 1.85 × 10^{-10} m^2/s, and 3.33 × 10^{-11} m^2/s and at $\lambda = 12$ is 3.10 × 10^{-10} m^2/s, 1.92 × 10^{-10} m^2/s, and 1.91 × 10^{-10} m^2/s for py-PPO, tri-PPO, and pen-PPO respectively. D_{OH} increases as we increase the hydration level; this indicates a continuous network of water formation and enhances the OH^- diffusivity. At a lower hydration level (Figure 5a), tri-PPO has a higher OH^- diffusivity, while at a higher hydration level (Figure 5b), py-PPO has a higher OH^- diffusivity. According to eq 4, ion conductivity (σ) can be obtained directly from D_{OH}.[15] Taking tri-PPO as an example, ion conductivity increases as we increase the hydration level, at $\lambda = 3$, $\sigma = 33.7$ mS/cm, and at $\lambda = 12$, $\sigma = 67.10$ mS/cm. The same trend was observed by Liu et al.,[20] at $\lambda = 5.2$, $\sigma = 8.2$ mS/cm, and at $\lambda = 10.4$, $\sigma = 14.9$ mS/cm, also experimental results by Yang et al.,[21] and Ran et al.,[22] of the semicrystalline grafted PPO membranes showed the same trend, at lower hydration level ($\lambda = 6$), σ #x223c; 30 mS/cm, and at higher hydration level ($\lambda = 12$), σ #x223c; 87 mS/cm. This justifies our model to be reliable even though our current study only considers the vehicular mechanism for hydroxide transport.

https://doi.org/10.1021/acsomega.3c05291
ACS Omega 2023, 8, 48711−48718

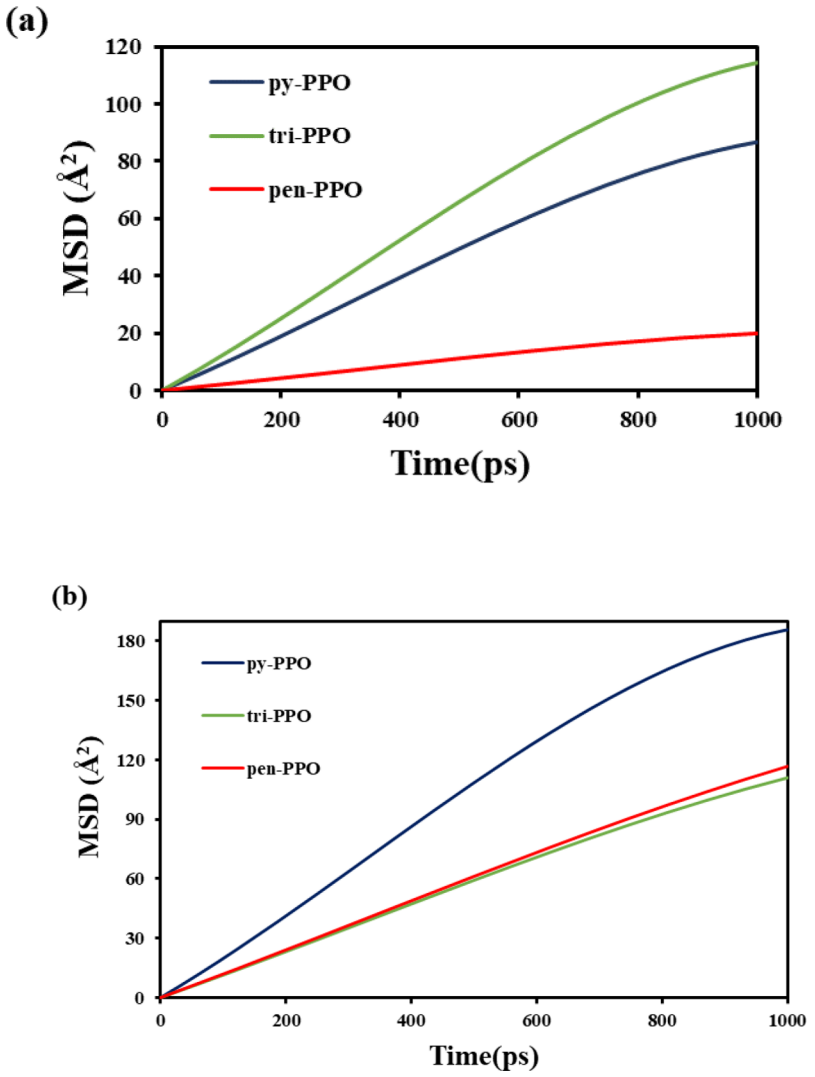

Figure 5. Mean square displacement of OH^- ions at (a) λ = 3, and (b) λ = 12.

3.2. Distribution of Water and Hydroxide around Different Azole Groups. Because water is responsible for transporting OH^- between adjacent cationic groups, understanding the hydration structure of cations helps study the effect of azole-based groups on OH^- transport.[3,4,15] The RDF peaks and CNs between cationic Nitrogen (N1) and the Oxygen atom of water molecules (Ow) ($g_{N1\text{-}Ow}(r)$) for tri-PPO are shown in Figure 6, between 2.9 and 5.5 Å, the RDF peaks decreases with an increase in hydration level, this is because of the rise in average water density in the membrane; according to eq 1, the RDF peak ($g_{A\text{-}B}(r)$) is inversely proportional to the average density of atoms in the cell (ρ).[15] At λ = 3, CNs of water molecules at the first solvation shell (2.9- 4.3 Å) is 2.03, at the second solvation shell (4.3- 5.5 Å) is 4.20, and the total is 6.23. At λ = 12, CNs of water molecules at the first solvation shell (2.9- 3.9 Å) is 1.98, at the second solvation shell (3.9- 5.5 Å) is 8.80, and the total is 10.8. We have more water molecules at higher hydration levels than at lower hydration levels, this explains why we have a higher diffusivity at higher hydration levels (λ = 12) for all AEMs than at lower hydration levels (λ = 3), as discussed in Section 3.1, since water facilitates OH^- transport. The same trend can be observed for py-PPO and pen-PPO, as shown in Figure S2.

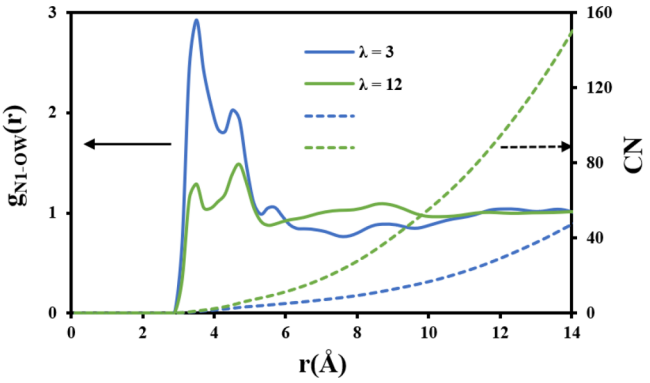

Figure 6. N1-Ow RDFs of tri-PPO at different hydration levels. (Solid lines represent the RDFs, and the dashed line represents the CNs).

Figures 7 and 8 show the cationic Nitrogen (N1) and the Oxygen atom of water molecules (Ow) ($g_{N1\text{-}Ow}(r)$) and the cationic Nitrogen (N1) and the Oxygen atom of hydroxide molecules (OH) ($g_{N1\text{-}OH}(r)$). To compare the distribution of water molecules between different AEMs, we computed their RDFs and CNs of $g_{N1\text{-}Ow}(r)$ at different hydration numbers,[3] as shown in Figure 7. Figure 7a shows RDFs and CN of different

https://doi.org/10.1021/acsomega.3c05291
ACS Omega 2023, 8, 48711−48718

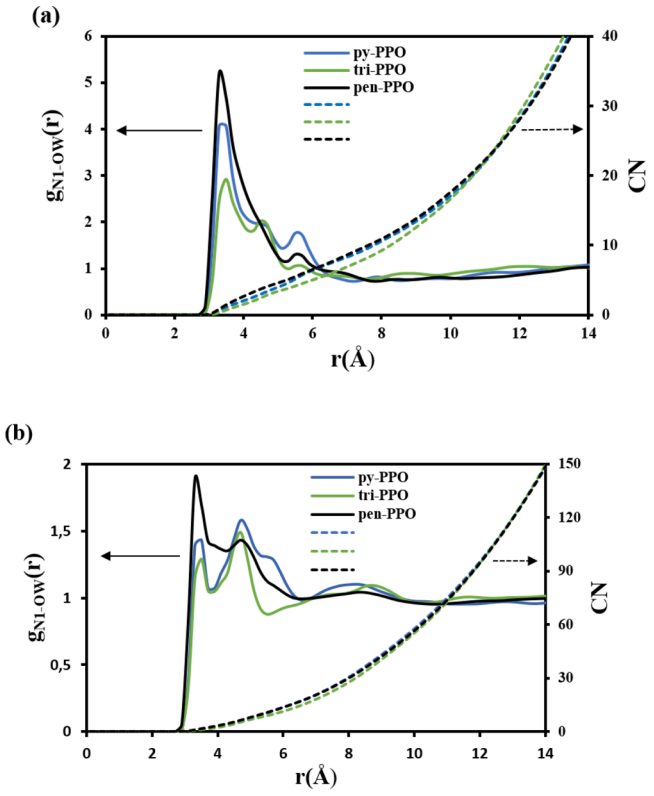

Figure 7. RDFs and CNs of different azole-based AEMs ($g_{N1\text{-}Ow}(r)$) at (a) λ = 3 and (b) λ = 12. (Solid lines represent the RDFs, and the dashed line represents the CNs).

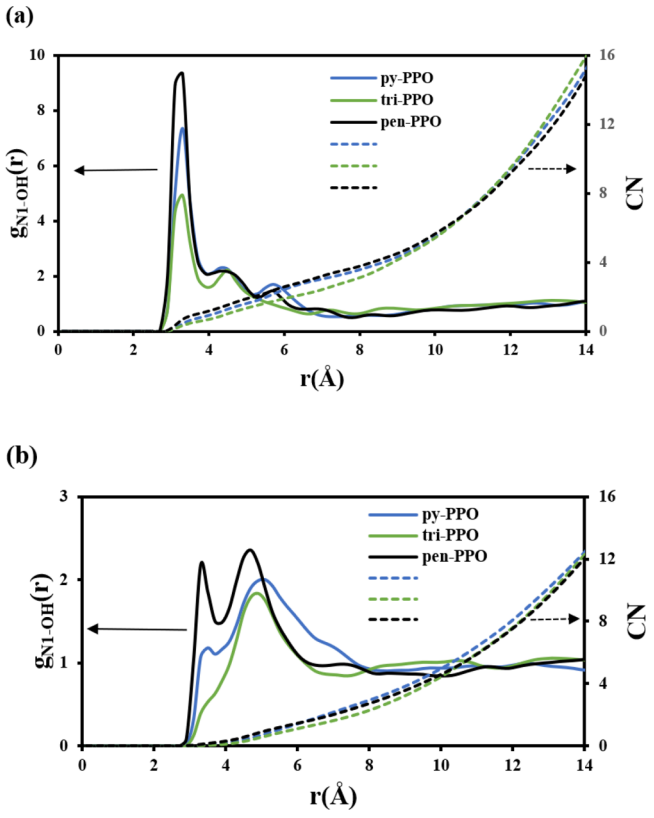

Figure 8. RDFs and CNs of different azole-based AEMs ($g_{N1\text{-}OH}(r)$) at (a) λ = 3 and (b) λ = 12. (Solid lines represent the RDFs, and the dashed line represents the CNs).

azole-based side chains at λ = 3, with two main peaks: the first hydration shell at 2.9−4.3 Å and the second hydration shell at 4.3−6.5 Å. CNs at the first hydration shell are 2.6, 2.0, and 3.3 for py-PPO, tri-PPO, and Pen-PPO, respectively. And at the second hydration shell, CNs are 7.4, 5.9, and 7.5 for py-PPO, tri-PPO, and Pen-PPO, respectively. At both hydration shells, pen-PPO has the highest water CNs, meaning that water molecules are strongly attracted to the cationic group of pen-PPO. Figure 7b shows RDFs and CN of different azole-based side chains at λ = 12, with two main peaks: the first hydration shell at 2.9−3.9 Å and the second hydration shell at 3.9−6.5 Å. CNs at the first hydration shell are 2.1, 1.9, and 2.9 for py-PPO, tri-PPO, and Pen-PPO, respectively. And at second hydration shell, CNs are 16.6, 14.4, and 16.8 for py-PPO, tri-PPO, and Pen-PPO, respectively. At both hydration shells, pen-PPO has the highest water CNs, which means water molecules are strongly attracted to the cationic group of pen-PPO.

To compare the distribution of OH^- ions around cationic groups between different AEMs, we computed their RDFs and CNs of $g_{N1\text{-}OH}(r)$ at different hydration numbers, as shown in Figure 8. This information is necessary, as mentioned in the Introduction that the major drawback in AEMs is the degradation of AEMs by the attack of OH^-. The membrane that is easily susceptible to OH^- attack will lose its cationic group due to Hofmann (or) E1 elimination reactions and nucleophilic substitution,[1,6,7] hence losing its hydroxide conductivity. Figure 8a shows RDFs and CN of different azole-based side chains at λ = 3, OH^- can easily approach pen-PPO, resulting in a higher RDF peak in the first hydration shell 2.5−4.5 Å and a higher number of OH^-. Also, Figure 8b shows RDFs and CN of different azole-based side chains at λ = 12, OH^- can easily approach pen-PPO, resulting in a higher RDF peak in the first hydration shell 2.9−8.1 Å and a higher number of OH^-. It is shown that few OH^- are in tri-PPO, and many are in pen-PPO in Figure 8a. The same trend is shown at a higher hydration level, as shown in Figure 8b. Hence, from the $g_{N1\text{-}Ow}(r)$ and $g_{N1\text{-}OH}(r)$ results, we expect pen-PPO to have low hydroxide conductivity at both hydration levels. These results agree with the hydroxide diffusivity results discussed in Section 3.1.

3.3. Distance between Functional Groups. OH^- pass through the overlapped area of the adjacent hydration shells during transportation, which is affected by the distance of adjacent cationic groups.[1] We calculate the distance between adjacent groups when CNs between N1−N1 equal 1.[15] The distance is between 6 and 9 Å for different AEMs at different hydration levels (Figure S3). As the λ increases, the distance between adjacent groups increases. This will reduce the D_{OH} of the AEMs because an increase in distances reduces the overlapping area making the path narrow and restricting efficient OH^- diffusion. As shown in Figure 9, at a lower hydration level, λ = 3, tri-PPO has the shortest distance, 6.1 Å, at CN = 1, and at a higher hydration level, λ = 12 py-PPO has a shorter distance. We should expect a higher diffusion in the membranes with the shortest distance between adjacent cationic groups because it means the macromolecules are densely packed[1] between the adjacent cationic groups and it can efficiently transport OH^-.These results agree with the hydroxide diffusivity results discussed in Section 3.1.

3.4. Water Cluster Analysis. The snapshots of the water cluster network in the py-PPO membrane are shown in Figure 10 for lower hydration levels (Figure 10a) and higher

https://doi.org/10.1021/acsomega.3c05291
ACS Omega 2023, 8, 48711−48718

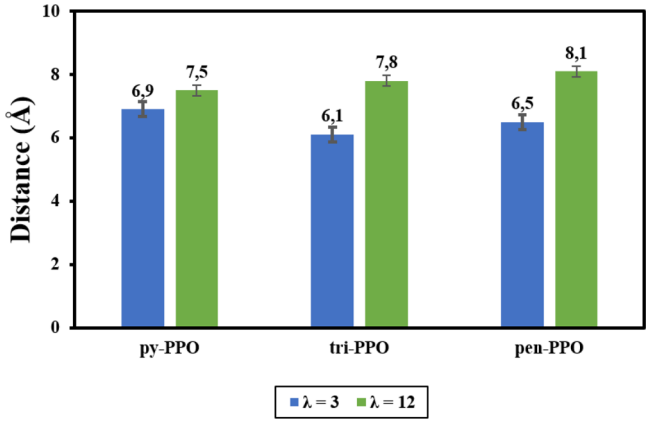

Figure 9. Distance between adjacent groups at different hydration levels.

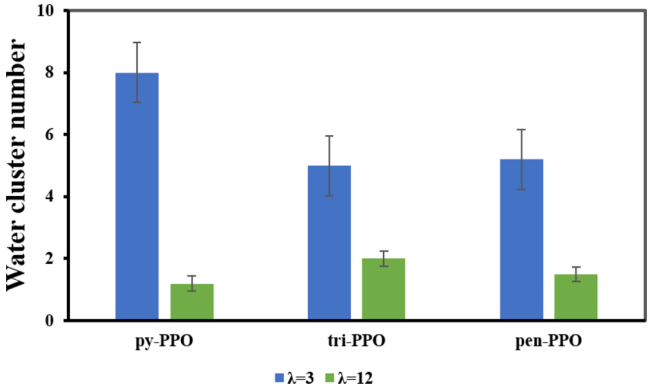

Figure 11. Cluster number (nanoseconds) of different azole-based AEMs at different hydration levels.

hydration levels (Figure 10b). Only hydroxide and water are shown, and the py-PPO chains are omitted. The clusters are shown in different colors, with the largest being green. At λ = 3, different small clusters can be observed, and at λ = 12, one large cluster can be seen. The membrane morphology is believed to exhibit a percolation transition from isolated hydrophilic water clusters to the three-dimensional network of water channels at λ = 12,[19] thus, we would expect a higher hydroxide diffusion at a higher hydration level. The same can be seen for other AEMs, as shown in Figures S4 and S5. These results agree with the hydroxide diffusivity results discussed in Section 3.1.

The connectivity of water clusters was explored by examining the average number of clusters—a smaller number of clusters results in larger connectivity, resulting in good ion transport, and vice versa. The oxygen−oxygen distance between water molecules and hydroxide ions in this study was set at 3.5 Å, roughly where the initial minimum in the oxygen−oxygen radial distribution functions for water molecules in bulk water is located.[18,19] As shown in Figure 11, the average number of clusters at lower hydration levels is 8.0, 5.0, and 5.2 for py-PPO, tri-PPO, and pen-PPO, respectively. Also, the average number of clusters at higher hydration levels is 1.2, 2.0, and 1.5 for py-PPO, tri-PPO, and pen-PPO, respectively. According to the definition of cluster analysis, the AEM with a smaller average number of clusters will result in better connectivity, promoting better OH^- transport. Therefore, from these results, a higher OH^- transport is expected for tri-PPO at λ = 3 and py-PPO at λ = 12. These results agree with the hydroxide diffusivity results discussed in Section 3.1.

4. CONCLUSIONS

The effect of different azole groups on OH^- transport in hydrated azole-based PPO AEMs was investigated by MD simulation. D_{OH} increases as we increase the hydration level; this indicates a continuous network of water formation and enhances the OH^- diffusivity. At a lower hydration level (λ = 3), tri-PPO has a higher OH^- diffusivity, while at a higher hydration level (λ = 12), py-PPO has a higher OH^- diffusivity. Moreover, pen-PPO has the lowest diffusivity at both hydration levels. The major drawback in AEMs is the degradation of AEMs by the attack of OH^-. The membrane that is easily susceptible to OH^- attack will lose its cationic group due to Hofmann (or) E1 elimination reactions and nucleophilic substitution, hence losing its hydroxide conductivity. To compare which AEMs are susceptible to OH^- attack, we computed RDFs and CNs for $g_{N1\text{-}OH}(r)$. At λ = 3, OH^- can easily approach pen-PPO, and also at λ = 12, OH^- can easily approach pen-PPO; these results of $g_{N1\text{-}Ow}(r)$ and $g_{N1\text{-}OH}(r)$ show we would expect pen-PPO to have a low hydroxide conductivity at both hydration levels, which agrees with the diffusivity values obtained. OH^- pass through the overlapped area of the adjacent hydration shells during transportation, which is affected by the distance of adjacent cationic groups, an increase in distances reduces the overlapping area making the path narrow and restricting efficient OH^- diffusion. From our results, at a lower hydration level, λ = 3, tri-PPO has the shortest distance, 6.1 Å at CN = 1, and at a

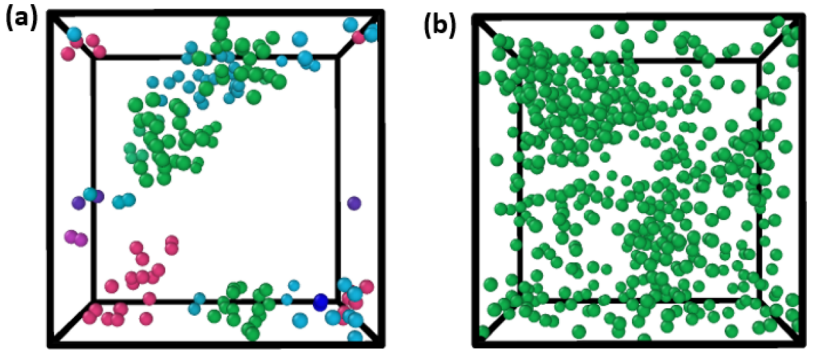

Figure 10. Snapshots of py-PPO water clusters at (a) λ = 3 and (b) λ = 12. Each cluster is shown in a different color (with the largest being green), and the py-PPO chains are not shown.

https://doi.org/10.1021/acsomega.3c05291
ACS Omega 2023, 8, 48711−48718

higher hydration level, $\lambda = 12$, pen-PPO has a shorter distance. This agrees with the D_{OH} results obtained from this study. The average number of clusters at lower hydration levels ($\lambda = 3$) is 8.0, 5.0, and 5.2 for py-PPO, tri-PPO, and pen-PPO, respectively. Also, at $\lambda = 12$, the average number of clusters at higher hydration levels is 1.2, 2.0, and 1.5 for py-PPO, tri-PPO, and pen-PPO, respectively. According to the definition of cluster analysis, the AEM with a smaller average number of clusters will result in better connectivity, promoting better OH^- transport. Therefore, from these results, a higher OH^- transport is expected for tri-PPO at $\lambda = 3$ and py-PPO at $\lambda = 12$. These results agree with the diffusivity results. These results give theoretical guidance on the design of azole-based AEMs which can be applied as a guide toward designing an AEM with good properties and water management in a practical setting.

■ ASSOCIATED CONTENT

Supporting Information

The Supporting Information is available free of charge at https://pubs.acs.org/doi/10.1021/acsomega.3c05291.

(Figure S1) OH^- diffusivities of pen-PPO at different hydration levels, (Figure S2) N1-Ow RDFs and CNs of py-PPO and pen-PPO at different hydration levels, (Figure S3) Distance between adjacent cationic groups at $\lambda = 3$ and $\lambda = 12$, (Figure S4) Snapshots of tri-PPO water clusters for at $\lambda = 3$ and $\lambda = 12$, (Figure S5) Snapshots of pen-PPO water clusters for at $\lambda = 3$ and $\lambda = 12$ (PDF)

■ AUTHOR INFORMATION

Corresponding Authors

Takuya Mabuchi − *Frontier Research Institute of Interdisciplinary Sciences, Tohoku University, Sendai, Miyagi 9808577, Japan; Institute of Fluid Science, Tohoku University, Sendai, Miyagi 980-8577, Japan;* orcid.org/0000-0001-8253-4273; Email: mabuchi.@tohoku.ac.jp

Phumlani F. Msomi − *Department of Chemical Science and Research Centre for Synthesis and Catalysis, Department of Chemical Science, University of Johannesburg, 2028 Johannesburg, South Africa;* orcid.org/0000-0003-4900-9009; Email: pmsomi@uj.ac.za

Author

Thabakgolo T. Letsau − *Department of Chemical Science and Research Centre for Synthesis and Catalysis, Department of Chemical Science, University of Johannesburg, 2028 Johannesburg, South Africa*

Complete contact information is available at: https://pubs.acs.org/10.1021/acsomega.3c05291

Author Contributions

All authors contributed equally.

Funding

We thank the University of Johannesburg for funding and we also thankful for funding from IRG - Japan Society for the Promotion of Science/NRF Research Cooperation Programme (Grant number 132994).

Notes

The authors declare no competing financial interest.

■ ACKNOWLEDGMENTS

All the authors acknowledge the University of Johannesburg for lab space and National Research Fund (NRF) for its financial assistance. Authors also thank the Japan Society for the Promotion of Science/NRF Research Cooperation Programme (Grant number 132994) for funding. Authors also thank Frontier Research Institute of Interdisciplinary Sciences, Tohoku University for computation training and visit.

■ REFERENCES

(1) Song, B.; Li, D.; He, Y.; Huang, D.; Tong, Z. Molecular dynamics simulation of alkaline electrolyte diffusion in anion exchange membrane. *Sci. China Technol. Sci.* **2020**, *63*, 2241−2255.

(2) Zhang, W.; van Duin, A. C. T. ReaxFF Reactive Molecular Dynamics Simulation of Functionalized Poly(phenylene oxide) Anion Exchange Membrane. *Journal of physical chemistry. C* **2015**, *119*, 27727−27736.

(3) Han, K. W.; Ko, K. H.; Abu-Hakmeh, K.; Bae, C.; Sohn, Y. J.; Jang, S. S. Molecular Dynamics Simulation Study of a Polysulfone-Based Anion Exchange Membrane in Comparison with the Proton Exchange Membrane. *Journal of physical chemistry. C* **2014**, *118*, 12577−12587.

(4) Merinov, B. V.; Goddard, W. A. Computational modeling of structure and OH-anion diffusion in quaternary ammonium polysulfone hydroxide − Polymer electrolyte for application in electrochemical devices. *Journal of membrane science* **2013**, *431*, 79−85.

(5) Hagesteijn, K.; Jiang, S.; Ladewig, B. A review of the synthesis and characterization of anion exchange membranes. *J. Mater. Sci.* **2018**, *53*, 11131−11150.

(6) Msomi, P.; Nonjola, P.; Ndungu, P.; Ramontja, J. Quaternized poly (2,6 dimethyl−1,4 phenylene oxide)/polysulfone blended anion exchange membrane for alkaline fuel cells application. *Materials Today: Proceedings* **2018**, *5*, 10496−10504.

(7) Vijayakumar, V.; Nam, S. Y. Recent advancements in applications of alkaline anion exchange membranes for polymer electrolyte fuel cells. *Journal of industrial and engineering chemistry (Seoul, Korea)* **2019**, *70*, 70−86.

(8) Dang, H.; Jannasch, P. A comparative study of anion-exchange membranes tethered with different hetero-cycloaliphatic quaternary ammonium hydroxides. *Journal of materials chemistry. A, Materials for energy and sustainability* **2017**, *5*, 21965−21978.

(9) Gu, L.; Dong, H.; Sun, Z.; Li, Y.; Yan, F. Spirocyclic quaternary ammonium cations for alkaline anion exchange membrane applications: An experimental and theoretical study. *RSC Adv.* **2016**, *6*, 94387−94398.

(10) Vijayakumar, V.; Son, T. Y.; Im, K. S.; Chae, J. E.; Kim, H. J.; Kim, T. H.; Nam, S. Y. Anion Exchange Composite Membranes Composed of Quaternary Ammonium-Functionalized Poly(2,6-dimethyl-1,4-phenylene oxide) and Silica for Fuel Cell Application. *ACS omega* **2021**, *6*, 10168−10179.

(11) Arges, C. G.; Ramani, V. Two-dimensional NMR spectroscopy reveals cation-triggered backbone degradation in polysulfone-based anion exchange membranes. *Proceedings of the National Academy of Sciences - PNAS* **2013**, *110*, 2490−2495.

(12) Bakangura, E.; He, Y.; Ge, X.; Zhu, Y.; Wu, L.; Ran, J.; Cheng, C.; Emmanuel, K.; Yang, Z.; Xu, T. Tetrazole tethered polymers for alkaline anion exchange membranes. *Front. Chem. Sci. Eng.* **2018**, *12*, 306−310.

(13) Irannejad, H. Nitrogen Rich Heterocycles as a Privileged Fragment in Lead Discovery. *Med. Anal. Chem. Int. J.* **2018**, *2*, 1 DOI: 10.23880/macij-16000125.

(14) Li, N.; Guiver, M. D.; Binder, W. H. Towards High Conductivity in Anion-Exchange Membranes for Alkaline Fuel Cells. *ChemSusChem* **2013**, *6*, 1376−1383.

(15) Wu, L.; Zhou, X.; Zhang, G.; Zhang, N.; Huang, Y.; Dai, S.; Shen, Y. Tunable OH^- Transport and Alkaline Stability by Imidazolium-Based Groups of Poly(2,6-dimethyl-1,4-phenylene oxide) Anion Exchange Membranes: A Molecular Dynamics Simulation. *Ind. Eng. Chem. Res.* **2021**, *60*, 2481.
(16) Chen, C.; Tse, Y. S.; Lindberg, G. E.; Knight, C.; Voth, G. A. Hydroxide Solvation and Transport in Anion Exchange Membranes. *J. Am. Chem. Soc.* **2016**, *138*, 991−1000.
(17) Hori, Y.; Suetake, T.; Shiota, Y.; Yoshizawa, K.; Shigeta, Y.; Ida, T.; Mizuno, M. Local Structures and Dynamics of Imidazole Molecules in Poly(vinylphosphonic acid)−Imidazole Composite Investigated by Molecular Dynamics. *ACS Appl. Polym. Mater.* **2020**, *2*, 1561.
(18) Mabuchi, T.; Tokumasu, T. Effect of bound state of water on hydronium ion mobility in hydrated Nafion using molecular dynamics simulations. *J. Chem. Phys.* **2014**, *141*, 104904.
(19) Mabuchi, T.; Tokumasu, T. Relationship between Proton Transport and Morphology of Perfluorosulfonic Acid Membranes: A Reactive Molecular Dynamics Approach. *journal of physical chemistry. B* **2018**, *122*, 5922−5932.
(20) Liu, L.; He, S.; Zhang, S.; Zhang, M.; Guiver, M. D.; Li, N. 1,2,3-Triazolium-Based Poly(2,6-Dimethyl Phenylene Oxide) Copolymers as Anion Exchange Membranes. *ACS applied materials & interfaces* **2016**, *8*, 4651−4660.
(21) Yang, J.; Liu, C.; Hao, Y.; He, X.; He, R. Preparation and investigation of various imidazolium-functionalized poly(2,6-dimethyl-1,4-phenylene oxide) anion exchange membranes. *Electrochimica acta* **2016**, *207*, 112−119.
(22) Ran, J.; Wu, L.; Varcoe, J. R.; Ong, A. L.; Poynton, S. D.; Xu, T. Development of imidazolium-type alkaline anion exchange membranes for fuel cell application. *Journal of membrane science* **2012**, *415−416*, 242−249.

https://doi.org/10.1021/acsomega.3c05291
ACS Omega 2023, 8, 48711−48718